

# Effective hamiltonian for FeAs based superconductors

Efstratios Manousakis<sup>(1,2)</sup>, Jun Ren<sup>(3)</sup> and Efthimios Kaxiras<sup>(3)</sup>

<sup>(1)</sup>*Department of Physics and MARTECH, Florida State University, Tallahassee, FL 32306-4350, USA*

<sup>(2)</sup>*Department of Physics, University of Athens, Panepistimioupolis, Zografos, 157 84 Athens, Greece*

<sup>(3)</sup>*Department of Physics and School of Engineering and Applied Sciences, Harvard University, Cambridge, MA 02138, USA*

(Dated: June 21, 2024)

The recently discovered FeAs-based superconductors show intriguing behavior and unusual dynamics of electrons and holes which occupy the Fe  $d$ -orbitals and As  $4s$  and  $4p$  orbitals. Starting from the atomic limit, we carry out a strong coupling expansion to derive an effective hamiltonian that describes the electron and hole behavior. The hopping and the hybridization parameters between the Fe  $d$  and As  $s$  and  $p$ -orbitals are obtained by fitting the results of our calculations based on the local density approximation to a tight-binding model which involves these as fitting parameters. We find that the effective hamiltonian, in the strong on-site Coulomb repulsion limit, consists of three parts which operate on three distinct sub-spaces coupled through Hund's rule. The three sub-spaces describe different components (or subsystems): (a) one spanned by the degenerate atomic Fe orbitals  $d_{xz}$  and  $d_{yz}$ ; (b) one spanned by the atomic Fe orbitals  $d_{xy}$  and  $d_{z^2}$ ; and (c) one spanned by the  $d_{x^2-y^2}$  Fe orbital. Each of these hamiltonians is an extended  $t - t' - J - J'$  model and is characterized by different coupling constants and filling factors. For the case of the undoped material we argue that the first component alone prefers a ground state characterized by a spin-density-wave order similar to that observed in recent experimental studies, while the other two subspaces prefer an antiferromagnetic order. We also argue that the observed spin-density-wave order serves as a compromise state that minimizes the ground state energy of the total hamiltonian.

PACS numbers: 74.70.-b,74.25.Ha,74.25.Jb,75.10.-b

## I. INTRODUCTION

The recent observation of superconductivity in quaternary oxypnictides<sup>1,2,3,4,5,6</sup>, which are materials based on FeAs (and FeP), has rekindled intense activity<sup>7,8,9,10,11,12,13,14,15,16,17,18,19,20,21,22,23,24</sup> to find a description of the strong electronic correlations present in these materials and in the cuprates which could be responsible for such phenomena.

The structure of the new materials<sup>2</sup> (Fig. 1) consists of FeAs layers sandwiched between two LaO layers with rather weak interlayer coupling. The FeAs layers consists of a square lattice formed by the Fe atoms, while the As atoms, which sit just above and just below the plane (see Fig. 1), form FeAs<sub>4</sub> octahedra squeezed along the  $c$  axis such that each Fe-As bond forms a  $\pm 30^\circ$  angle with the Fe plane.

As a function of temperature, the resistivity of the undoped parent compound, which is not an insulator, shows a drop around 150 K<sup>2,25</sup> before turning back up below 50 K. In addition, the magnetic susceptibility also shows an anomaly at 150 K and it was argued<sup>25</sup> that the parent material has a spin-density-wave (SDW) instability below 150 K. Recent neutron diffraction studies<sup>26</sup> demonstrate that the parent compound at 150 K undergoes a structural distortion from tetragonal at high temperature to monoclinic at low temperature. Furthermore, these neutron diffraction studies show that below  $\sim 134$  K, while in the monoclinic phase, it develops a SDW order shown in Fig. 1. Subsequent Mössbauer and  $\mu$ SR studies<sup>27</sup> confirm these findings and more precisely the structural transition is found to be around 156 K and

the magnetic transition around 138 K. The structural distortion which brings about the monoclinic structure at low temperature is such that the rows of atoms which have their spins antiferromagnetically aligned are closer as compared to the rows of atoms in the perpendicular direction.

The electronic structure of the LaO<sub>1-x</sub>F<sub>x</sub>FeAs has been studied by density functional theory<sup>7,11</sup> and by dynamical mean field theory<sup>9</sup>. There are arguments to rule out phonon-mediated superconductivity<sup>9,10</sup> in LaO<sub>1-x</sub>F<sub>x</sub>FeAs. In addition, there are suggestions that a two-band model<sup>12,13,14,15,18</sup> may be the right effective hamiltonian to use in order to describe the low energy physics of these materials.

Since the interlayer coupling is found to be weak<sup>11</sup>, in order to provide a simpler basis to understand the electronic structure of these materials we will consider a single FeAs layer. In order to provide further justification for the above statement, we calculated the band structure of LaOFeAs and also that of a single FeAs layer using the local density approximation (LDA) and we find the important features of the bands near the Fermi level obtained by the two calculations are essentially the same, including relative position to the Fermi level and overall dispersion features. Accordingly, our starting point is a hamiltonian which includes the five Fe  $d$ -orbitals and four outer As orbitals ( $4s$  and  $4p$ ). We include both direct Fe-Fe hopping as well as hybridization between the Fe  $d$  and the As  $4s$  and  $4p$  orbitals. In addition, we include the local Coulomb repulsion energy for adding an electron on any of the Fe  $d$  states via Hubbard-type terms in the hamiltonian and coupling through Hund's rule.

We determine the relative energy of the atomic orbitals as well as the hopping and the hybridization matrix elements as follows: We carry out a set of first-principles calculation based LDA of the electronic structure of a single FeAs layer. Using as basis the above mentioned nine states we fit the results of the LDA calculation using the tight-binding approximation to determine the values of the hopping matrix elements and the local energy levels. We find that the energy difference between the atomic orbitals is less than 1 eV while the Coulomb repulsion to add two electrons on the same Fe  $d$  orbital is much larger (of the order of 5 eV). Therefore, we follow the band structure calculation with a strong coupling expansion in which the hopping and hybridization terms are used as perturbation. We systematically derive a low energy effective hamiltonian to describe this multi-band system.

Through this analysis, we show that the relevant low energy degrees freedom can be described by two two-“flavor” subsystems, one in which the two flavors correspond to electrons in the  $d_{xz}$  and  $d_{yz}$  states of the Fe atoms and another in which the two flavors correspond to  $d_{xy}$  and  $d_{z^2}$  Fe orbitals, and a third one-flavor subsystem corresponding to the  $d_{x^2-y^2}$  orbital, with each subsystem described by a  $t-t'-J-J'$  model where the spin degrees of freedom of all three subsystems couple through Hund’s rule. Using this hamiltonian we are able to explain why the undoped material orders in the SDW pattern shown in Fig. 1 as reported by recent neutron scattering experiments<sup>26</sup>.

The paper is organized as follows: Section II gives a detailed discussion of our density-functional-theory band structure calculations. Section III presents the strong-limit analysis which leads to the effective hamiltonian. Section IV gives a discussion of the physics of the effective hamiltonian, and the nature of superconducting behavior that our model produces.

## II. RESULTS OF THE LDA AND TIGHT-BINDING APPROXIMATION

Our first-principles calculations are performed within the framework of density functional theory (DFT) using the SIESTA code<sup>28</sup>. The reason for choosing this particular method is that it employs a localized basis of atomic-like orbitals for the expansion of the wavefunctions which makes the interpretation of electronic wavefunctions in the solid straightforward and transparent, without the need for additional analysis such as projection to localized Wannier-type orbitals.

We use pseudopotentials of the Troullier-Martins type<sup>29</sup> to represent the interaction between valence electrons and ionic cores, and the Ceperley-Alder form of the local density approximation for the exchange-correlation functional<sup>30</sup>. The unit cell for the simplified model system, a single FeAs layer, contains two Fe and two As atoms with a vacuum layer with thickness  $\sim 19$  Å. The

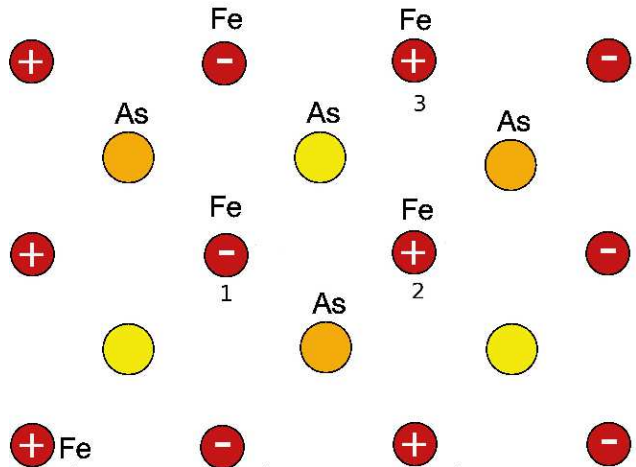


FIG. 1: The structure of the FeAs layer in the FeAs based superconductors. The Fe atoms form a square lattice. The As atoms above (orange) and below (yellow) the plane formed by the Fe atoms form two square sublattices one just above and the other just below the Fe plane. The plus and - signs on the Fe atoms denote the spin orientation observed in the neutron scattering experiment<sup>26</sup>. The various labels will be used below to explain the various types of antiferromagnetic exchange interactions.

full system, bulk LaOFeAs has two atoms of each type (Fe, As, La and O) in the unit cell. We choose an auxiliary real space grid equivalent to a plane-wave cutoff of 100 Ry, and use  $8 \times 8 \times 1$  Monkhorst-Pack k-point grid for the FeAs layer,  $4 \times 4 \times 1$  for the  $(2 \times 2)$  FeAs supercell, and a  $8 \times 8 \times 4$  grid for the LaOFeAs structure. For geometry optimization, a structure is considered fully relaxed when the magnitude of forces on all atoms is smaller than 0.04 eV/Å.

LaOFeAs, belonging to the tetragonal  $P4/nmm$  space group, has a layered structure<sup>2</sup>. The FeAs layer serves as the carrier conduction channel and it has strong electronic couplings within the layer. For the FeAs layer, the total energy of the antiferromagnetic (AFM) ground state is lower by 80 meV per unit cell than that of ferromagnetic (FM) state, suggesting that, within our DFT-LDA calculation, the AFM phase is preferred within the FeAs layer. The corresponding lattice constants are calculated to be  $a = 3.95$  Å for the AFM phase. The calculated band structure along the  $\Gamma$ -X-M- $\Gamma$  direction in the reciprocal space is shown in Fig. 2(b). A complex band structure is shown, with several electron bands around the Fermi level. Since introduction of electron doping is necessary in order to produce superconductivity in LaOFeAs-based materials, we focus only on the five unoccupied states above the Fermi level in the following. Note that hole-doping induced superconductivity in the materials has been also reported recently<sup>6</sup>. These unoc-

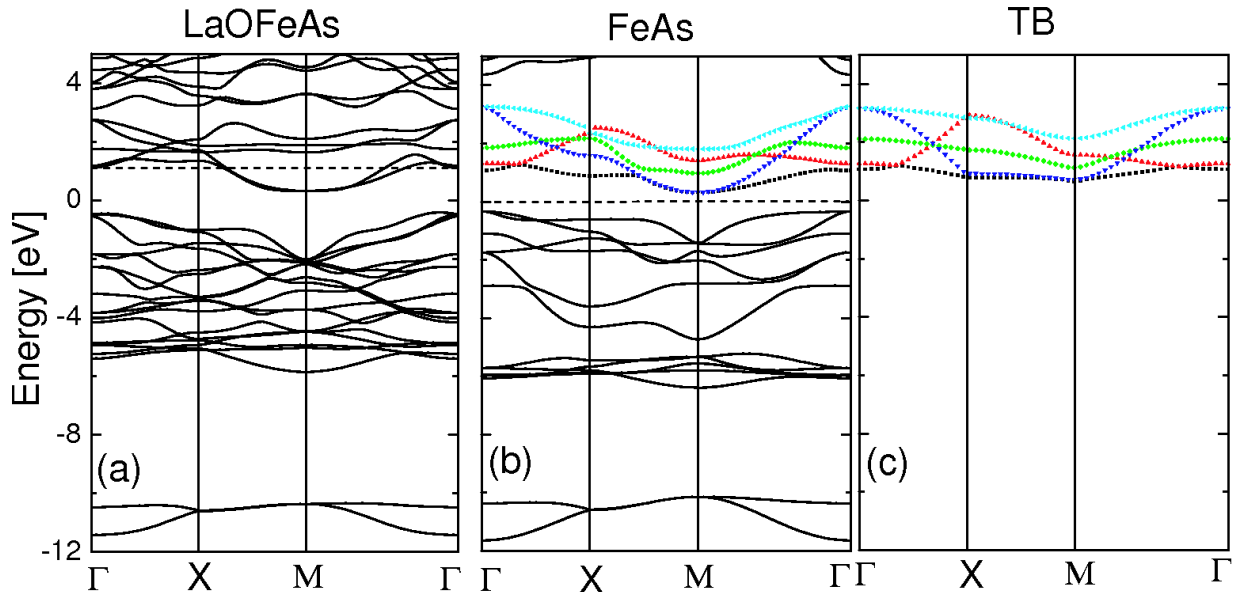


FIG. 2: The band structure of: (a) the LaOFeAs compound and (b) the FeAs plane only, both from the DFT/ LDA calculation; (c) the tight-binding approximation results for the five bands discussed in the text. The dashed line shows the Fermi level.

occupied electronic orbitals are shown with different colors and symbols. By analyzing the character of the wavefunctions at the center of the Brillouin Zone ( $\Gamma$  point), we identify these five bands as the  $3d_{xy}$ ,  $3d_{z^2}$ ,  $3d_{x^2-y^2}$ ,  $3d_{xz}$ , and  $3d_{yz}$  orbitals, counting from lower energy to higher. The distinct character of the five orbitals will determine the coupling strength between doped electrons in these states.

The use of the single FeAs layer as a simplified model for the study of superconductivity in LaOFeAs is justified by the electronic structure calculations for the bulk material. The optimal lattice constants for bulk LaOFeAs are  $a = 4.03552 \text{ \AA}$ , and  $c = 8.7393 \text{ \AA}$ . The relevant band structure is plotted in Fig. 2(a). Comparing to the band structure of the FeAs layer (Fig. 2(b)) in the same energy region, we find that the essential features of all the important bands near the Fermi level are the same, including position of the bands relative to the Fermi level and overall dispersion. In particular, the two lowest occupied states for both structures are almost the same. In addition, there are exactly five states around the Fermi level in the band structure of LaOFeAs, the ones contributed by the FeAs layer. The difference is that each band is composed of two or more orbital combinations from different Fe and As atoms in bulk LaOFeAs, while the bands can be identified almost purely with one atomic orbital

in the FeAs layer. Due to the presence of the LaO layers, the Fermi level has moved to higher values so that the two lowest unoccupied states of the FeAs layer become partially occupied by extra electrons contributed from the LaO layers.

We considered different spin configurations in the AFM phase. For this calculation we use a  $(2 \times 2)$  FeAs supercell. The two spin configurations are: (i) AFM1, which is simply repetition of the spin configuration in the  $(1 \times 1)$  unit cell; (ii) AFM2, which has the same spin alignment in one of the two diagonal directions of the Fe lattice and alternating spins along the other direction, as shown in Fig. 1. The total energy for the former symmetry is lower by 0.95 eV per  $(2 \times 2)$  cell, suggesting the AFM1 configuration of spins is more stable than the AFM2 one. This result may be due to the fact that our calculation is for the charge neutral FeAs layer, where the Fermi level falls below that of the complete LaOFeAs structure; namely, in the FeAs layer case, iron is in  $\text{Fe}^{3+}$  state, while in LaOFeAs iron is in the  $\text{Fe}^{2+}$  state. Our goal is to calculate a tight-binding hamiltonian which approximately gives the same band structure as that of the LaOFeAs (or the FeAs layer) more or less independently of the filling factor (i.e., the position of the Fermi level). Namely, the hopping matrix elements, needed for the hamiltonian upon which the strong coupling expansion will be based,

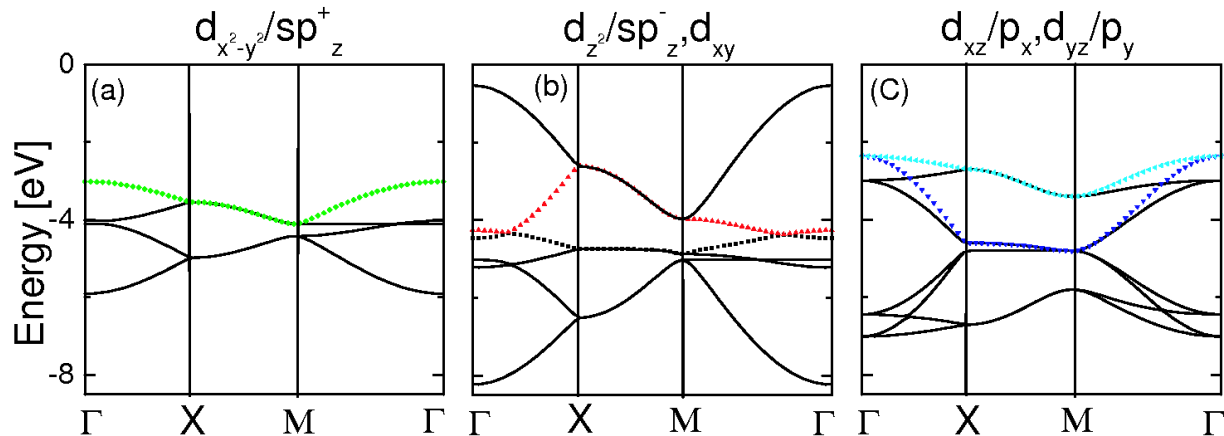


FIG. 3: The band structure of FeAs obtained from the tight-binding approximation. The states are separated into three groups: (a) the Fe  $d_{x^2-y^2}$ /As  $sp_z^+$  group; (b) the Fe  $d_{z^2}$ /As  $sp_z^-$  and Fe  $d_{xy}$  group; (c) the Fe  $d_{xz}$ /As  $p_x$  and Fe  $d_{yz}$ /As  $p_y$  group. The bands from each group that constitute the five-band space shown in Fig. 2(c) are highlighted in the same color coding.

are not expected to be significantly affected by the value of the filling factor. As it will become evident in the next paragraph and by comparing Fig. 2(b) with Fig. 2(c) we have achieved this goal. Therefore, we calculated the LaOFeAs structure in the AFM1 spin configuration.

Within the tight-binding (TB) approximation, we investigated in detail the hybridization between the five  $3d$  orbitals of Fe, and the four  $4s$ ,  $4p$  orbitals of As. The resulting 18 bands of the FeAs layer (there are 2 Fe and 2 As atoms in the  $(1 \times 1)$  unit cell) are shown in Fig. 3. We limit our model to include only the hopping and hybridization between the nearest Fe-Fe and Fe-As atoms. Due to the different nature of these couplings and geometrical constraints, we can divide the corresponding interactions into three separate matrices assuming the coupling between them is negligible. Fig. 3(a) represents the result of the mixing between any  $3d_{x^2-y^2}$  of the nearest neighbor Fe atoms and the hybridization of  $4s$  and  $4p_z$  orbitals of the nearest As atoms. Comparing these four bands with the band structure calculated using DFT/LDA, we identify the fourth curve (green line) as the one of the five unoccupied states in Fig. 2(c). Similarly, the band structure for the subspace spanned by the Fe  $3d_{z^2}$  orbitals, the As  $4sp_z$  hybridized orbitals, and the Fe  $3d_{xy}$  orbitals, is shown in Fig. 3(b). The red and

black lines of the band structure above the Fermi level (in Fig. 2(b)) are primarily composed of contributions from the Fe  $d_{z^2}$  orbitals, the As  $sp_z$  and the Fe  $d_{xy}$  orbitals. The bands corresponding to the two degenerate states,  $3d_{xz}$  and  $3d_{yz}$  of Fe, and their coupling with the  $4p_x$  and  $4p_y$  of the nearest As atoms are shown in Fig. 3(c). The two light blue and dark blue curves are referred to as the two degenerate unoccupied states. It is clear that our TB results for the FeAs layer, with the selected orbitals shown in Fig. 2(c), are in good agreement with the LDA calculation in Fig. 2(b). The parameters of the fit of our TB approximation are given in Tables I, II and III and are explained in the following section in terms of the parameters of our more general hamiltonian.

### III. STRONG COUPLING LIMIT

Let us consider the hamiltonian describing a single FeAs layer of Fe and As (or P) atoms:

$$\hat{H} = \hat{H}_a + \hat{T} + \hat{U} \quad (1)$$

with the three terms defined by:

$$\hat{H}_a = \sum_{i,\nu,\sigma} \epsilon_d(\nu) d_{i\sigma}^{(\nu)\dagger} d_{i\sigma}^{(\nu)} + \sum_{l,\alpha,\sigma} \epsilon_{sp}(\alpha) sp_{l\sigma}^{(\alpha)\dagger} sp_{l\sigma}^{(\alpha)} \quad (2)$$

$$\hat{T} = - \sum_{\langle ij \rangle, \sigma, \nu \nu'} (t_{\nu \nu'} d_{j\sigma}^{(\nu')\dagger} d_{i\sigma}^{(\nu)} + h.c) - \sum_{i, \sigma, \nu, \alpha} \sum_{l(i)} (V_{il}^{\nu\alpha} d_{i\sigma}^{(\nu)\dagger} sp_{l\sigma}^{(\alpha)} + h.c) \quad (3)$$

$$\hat{U} = \sum_{\nu} U_{\nu}^{(d)} \sum_i n_d^{\nu}(i \uparrow) n_d^{\nu}(i \downarrow) + \sum_{\nu} U_{\nu}^{(sp)} \sum_i n_{sp}^{\nu}(i \uparrow) n_{sp}^{\nu}(i \downarrow) - \sum_{\nu, \nu'} J_{\nu, \nu'}^H \sum_i \vec{S}_d^{\nu}(i) \cdot \vec{S}_d^{\nu'}(i), \quad (4)$$

TABLE I: The on-site energies in eV for the Fe  $d$ -orbitals as determined by approximating the results of our LDA calculation using the tight-binding approximation discussed in Sec. II. In addition, the hopping matrix elements between two nearest neighbor Fe  $d$ -orbitals of the same type, i.e.,  $t_{\nu}$  are also given in this table. The notation is explained in Sec. III.

$\nu$	1	2	3	4	5
Fe $d$ -orbital	$d_{xy}$	$d_{xz}$	$d_{yz}$	$d_{x^2-y^2}$	$d_{z^2}$
$\epsilon_d(\nu)$	-4.74	-4.60	-4.60	-4.60	-4.10
$t_{\nu\nu}$	0.12	0.15	0.15	0.20	0.09

TABLE II: The on-site energies in eV for As  $sp$ -orbitals as determined by approximating the results of our LDA calculation using the tight-binding approximation discussed in Sec. II. Here  $sp_z^+$  and  $sp_z^-$  correspond to the linear combinations  $a|s\rangle + b|p_z\rangle$  and  $b|s\rangle - a|p_z\rangle$  of the As  $s$  and  $p_z$  orbitals respectively. The notation is explained in Sec. III.

$\alpha$	1	2	3	4
As $sp$ -orbital	$p_x$	$p_y$	$sp_z^+$	$sp_z^-$
$\epsilon_{sp}(\alpha)$	-4.80	-4.80	-5.02	-4.40

where the operator  $d_{i\sigma}^{(\nu)\dagger}$  creates an electron of spin  $\sigma$  on the  $\nu^{th}$  Fe  $d$ -orbital ( $\nu = 1, 2, 3, 4, 5$  is the index that corresponds to the five  $d$  Fe orbitals, i.e.,  $d_{xy}$ ,  $d_{xz}$ ,  $d_{yz}$ ,  $d_{x^2-y^2}$ , and  $d_{z^2}$  respectively) at the site  $i$  which has an energy  $\epsilon_d(\nu)$ . The operator  $sp_{l\sigma}^{(\alpha)\dagger}$  creates an electron of spin  $\sigma$  on the  $\alpha^{th}$  As which is one of the four outer orbitals, namely the two  $sp_z$ -orbitals and the  $p_x$  and  $p_y$  orbitals (thus,  $\alpha = 1, 2, 3, 4$  for the cases of  $4p_x, 4p_y$  and the  $a|s\rangle + b|p_z\rangle$  and  $b|s\rangle - a|p_z\rangle$  respectively) at the  $l^{th}$  As site and with corresponding site energy  $\epsilon_{sp}(\alpha)$ . The term  $V$  is the hybridization term between the Fe  $3d$  orbitals and the As orbitals. The sum over  $l(i)$  means that it is over all four As sites around the  $i^{th}$  Fe site. The hybridization matrix element  $V_{il}^{\nu\alpha}$  is proportional to the wave function overlap of the  $\nu^{th}$  Fe  $d$ -orbital and the As  $\alpha^{th}$   $sp$ -orbital. Some of these matrix elements are zero due to symmetry arguments and the most significant ones are of the order or less than 1 eV and are estimated in our tight binding approximation of the LDA results. Here  $n_d^{\nu}(i\sigma) = d_{i\sigma}^{(\nu)\dagger} d_{i\sigma}^{(\nu)}$  is the number operator and  $U_{\nu}^{(d,sp)}$  gives the Coulomb repulsion for pair of electrons placed on the same  $d$ -orbital or the same  $s$  or  $p$  As-orbital. The term proportional to  $J^H$  represents Hund's rule, with  $J^H > 0$ , of order less than 1 eV.

In Tables I,II and in Table III we give the non-zero matrix elements obtained by fitting the LDA results to

TABLE III: The hybridization matrix elements in eV for the Fe  $d$ - and As  $sp$ -orbitals as determined by approximating the results of our LDA calculation using a tight-binding approximation discussed in Sec. II. The notation is explained in Sec. III.

$V^{\nu\alpha}$	1( $d_{xy}$ )	2( $d_{xz}$ )	3( $d_{yz}$ )	4( $d_{x^2-y^2}$ )	5( $d_{z^2}$ )
1( $p_x$ )	0	1.0	0	0	0
2( $p_y$ )	0	0	1.0	0	0
3( $sp_z^+$ )	0	0	0	0.35	0
4( $sp_z^-$ )	0	0	0	0	0.95

the tight binding model (as explained in Sec. II) which includes the five Fe  $d$ -states and the four As  $sp$  states for each of the two Fe and the two As atoms in the  $\text{Fe}_2\text{As}_2$  unit cell and the matrix elements  $t_{\nu\nu'}$  and  $V^{\nu\alpha}$  between these states. In addition to the above terms, the tight-binding approximation to the LDA results gives two hopping matrix elements  $t_{\nu\nu'}$  for  $\nu \rightarrow d_{xz}$  and  $\nu' \rightarrow d_{yz}$ , which is  $t_{xz,yz} = 0.30$  eV for  $\nu \rightarrow d_{xy}$  and  $\nu' \rightarrow d_{z^2}$ , which is  $t_{xy,z^2} = 0.08$  eV. All other hopping matrix elements are either identically equal to zero due to symmetry or very small.

First we would like to note that the parameter  $U^d$  are of the order of 5 eV while the parameter  $U^{sp}$  is much smaller than that. Notice that the energy levels  $\epsilon_d(\nu)$  and  $\epsilon_{sp}(\nu)$  lie in the region  $-4.6 \pm 0.5$  eV, namely the energy difference between any pair of such states is less than 1 eV which is much smaller than the characteristic Coulomb repulsion energy  $U_d$ . Therefore, let us begin our analysis starting from the atomic or strong coupling limit. In this limit the unperturbed part of the hamiltonian  $\hat{H}_0$  is

$$\hat{H}_0 = \hat{H}_a + \hat{U} \quad (5)$$

and the hopping part  $\hat{T}$ , which includes the hybridization, plays the role of perturbation. The Fe and As ions in the FeAs plane of the undoped LaOFeAs parent compound are in the  $\text{Fe}^{2+}$  and in the  $\text{As}^{3-}$ . Therefore, the 5+4 states considered above are occupied by 14 electrons. The atomic configuration is shown in Fig. 4. Since we have more than 5 more electrons than levels, 5 energy levels must be doubly occupied. Since the  $d$  orbitals are much more costly as compared to the  $sp$  orbitals all 4 of the As orbital must be doubly occupied and the only doubly occupied  $d$  orbital is the  $d_{xy}$  which has the lowest energy. This is the only doubly occupied Fe  $d$ -orbital and the other four are singly occupied and the spin of these electrons are parallel because of Hund's rule, represented by the coupling  $J_H$ .

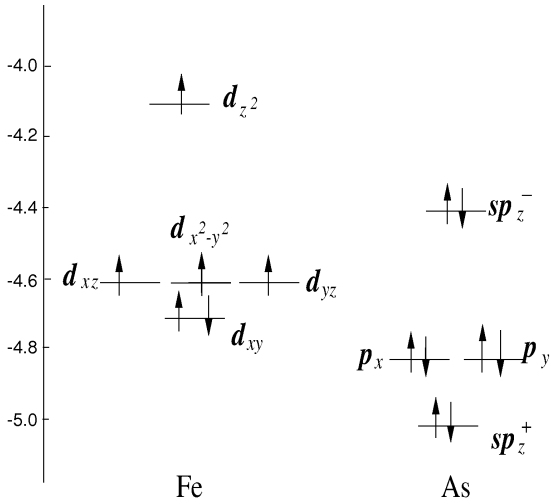


FIG. 4: The occupation of the  $\text{Fe}^{2+}$  and  $\text{As}^{3-}$  atomic levels in the FeAs plane of the undoped parent compound. The ordering of the levels is shown schematically, as obtained from the tight-binding approximation parameters.

Next we consider the effective hamiltonian which, in strong coupling perturbation theory, is given by

$$\hat{H}_{eff} = E_0 \hat{P}_0 + \hat{P}_0 \hat{T} \hat{\Omega}, \quad (6)$$

$$\hat{\Omega} = \hat{P}_0 + \hat{R}(\hat{T} \hat{\Omega} - \hat{\Omega} \hat{T}), \quad (7)$$

$$\hat{R} = \frac{\hat{Q}}{\hat{H}_0 - E_0}, \quad (8)$$

where  $E_0$  is the ground state energy given by the energy of the state depicted in Fig. 4. The  $\hat{H}_{eff}$  operates in the subspace  $S_0$  formed by the degenerate ground states of  $\hat{H}_0$ , i.e., the subspace of states produced by the direct product of atomic states like those in Fig. 4 in which the spins of the four electrons occupying the four  $d$ -orbitals, from one Fe atom to the next, point either all up or all down. The operator  $\hat{P}_0$  is a projection operator which projects into the subspace  $S_0$  and  $\hat{Q} = \hat{I} - \hat{P}_0$ , i.e., it is the operator which projects outside the subspace  $S_0$ . The above equation can be formally solved iteratively to yield the Rayleigh-Schrödinger expansion as a power series in  $\hat{T}$ . The leading term is  $\hat{T}$  which, when restricted in this subspace  $S_0$ , becomes just those direct Fe-Fe hopping terms, i.e.,

$$\hat{P}_0 \hat{T} \hat{P}_0 = - \sum_{\langle ij \rangle, \sigma, \nu \nu'} (t_{\nu \nu'} d_{j\sigma}^{(\nu')} \dagger d_{i\sigma}^{(\nu)} + h.c.), \quad (9)$$

and in the right-hand-side of the above equation we have omitted the projection operators if, from now on, we restrict ourselves to work in the subspace  $S_0$ .

Before we go on to discuss other second or higher order processes we would like to discuss the following important process. First of all direct hopping from any singly occupied  $d$  orbital to any other singly occupied  $d$  orbital of a nearest neighbor (nn) Fe atom (provided that they are antiferromagnetically aligned) is prohibited because of large energy cost  $U_d$ . However, if there is a non-zero hopping from the doubly occupied  $d_{xy}$  orbital to any other  $d$  orbital of a nn Fe atom, this process does not cost a significant amount of energy because the total number of doubly occupied  $d$  orbitals does not change through this process. This is indeed the case because the  $d_{xy}$  orbital couples to the  $d_{z^2}$  orbital. Let us consider the limit where  $U_\nu^d$  is independent of  $\nu$  and much larger than the energy level differences between the Fe-3d, As-4s or As-4p. In the zeroth order ground state the  $d_{xy}$  orbital is doubly occupied and in the above limit this double occupancy can move to the  $d_{z^2}$  orbital at a low energy cost because we do not change the number of doubly occupied orbitals. These types of processes, lead to what we term “off-diagonal” transitions, i.e., hopping or spin-exchange processes between two different type  $d$  orbitals of neighboring atoms. In addition, in order to include these processes we need to extend the calculation from the subspace  $S_0$  of degeneracy to a larger subspace in which the states are quasi-degenerate, namely to a subspace where we include all the states which have energy within the window  $\pm 0.5$  eV in which the atomic levels fall as already discussed. It is well-known and rather straightforward how to carry out such quasi-degenerate perturbation theory and find the effective hamiltonian. In the following in order to simplify the calculation we will take  $U_\nu^d$  to be independent of  $\nu$  and we will assume that  $U_\nu^d$  is much larger than the atomic energy level difference (which was found to be less than 1 eV within our TB approximation) and, in addition, we will take  $U^{(sp)} = 0$ .

First of all there are the familiar second order processes arising from the direct Fe-Fe hopping through the matrix elements  $t_{\nu\nu}$  which gives rise to an *antiferromagnetic exchange interaction* of the form

$$\mathcal{H}_{\nu,\nu} = J_{\nu,\nu} \sum_{\langle ij \rangle} \vec{S}_i^\nu \cdot \vec{S}_j^\nu, \quad (10)$$

$$J_{\nu,\nu} = \frac{4t_{\nu,\nu}^2}{U_d}. \quad (11)$$

In addition, we have antiferromagnetic coupling of the spins of two different type Fe  $d$ -orbitals due to the hopping terms  $t_{xz,yz}$  and  $t_{xy,z^2}$  which give rise to

$$\mathcal{H}_{\nu,\nu'} = J_{\nu,\nu'} \sum_{\langle ij \rangle} \vec{S}_i^\nu \cdot \vec{S}_j^{\nu'}, \quad (12)$$

$$J_{\nu,\nu'} = \frac{4t_{\nu,\nu'}^2}{U_d}, \quad (13)$$

where  $\nu, \nu'$  can be either  $xz, yz$  or  $xy, z^2$ . These processes take place only between nearest neighbors such as the Fe atoms 1 and 2 in Fig. 1.

As can be seen from Table III any particular Fe  $d$ -orbital  $\nu$  couples to only one As  $sp$ -orbital through a single hybridization coupling which for simplicity we call it  $V_\nu$  (with the exception of  $d_{xy}$  which couples to none). Specifically,  $V_1 = 0$ ,  $V_{2,3} = 1.0$  eV and stands for the hopping matrix elements  $d_{xz}$  (or  $d_{yz}$ )  $\rightarrow p_x$  (or  $\rightarrow p_y$ );  $V_4 = 0.35$  eV and corresponds to the matrix element  $d_{x^2-y^2} \rightarrow sp_z^+$ ;  $V_5 = 0.95$  eV and stands for the hopping  $d_{z^2} \rightarrow sp_z^-$ .

The next to leading order, beyond the first and second order discussed above, are fourth order processes involving an Fe  $d$ -orbital and the corresponding As  $sp$ -orbital with which it hybridizes. Let us consider, for example, the fourth order process involving  $V_2$  which leads to the familiar antiferromagnetic spin interaction<sup>31</sup>

$$\mathcal{H}_{22} = J_{22} \sum_{\langle ij \rangle} \vec{S}_i^2 \cdot \vec{S}_j^2, \quad (14)$$

$$J_{22} = 2b^2 \left[ \frac{1}{U_2^d} + \frac{1}{U_2^d + \epsilon} \right], \quad (15)$$

$$b = \frac{V_2^2}{U_2^d + \epsilon}, \quad (16)$$

where  $\epsilon \sim 0.2$  eV is the energy difference between the  $p_x$  As state and the  $d_{xz}$  Fe orbital. Since  $U_2^d \sim 5$  eV  $\epsilon$  can be neglected in the above expression and we find that

$$J_{22} \simeq \frac{4V_2^4}{U_2^d{}^3} \quad (17)$$

and we have limited ourselves to the case where  $U_\nu^d$  is independent of  $\nu$ . More generally, within the same approximation, we find that for two nn Fe atoms (such as Fe atoms 1 and 2 in Fig. 1) for any of the four  $d$ -orbitals, we obtain

$$\mathcal{H}_{\nu,\nu} = J_{\nu\nu} \sum_{\langle ij \rangle} \vec{S}_i^\nu \cdot \vec{S}_j^\nu, \quad (18)$$

$$J_{\nu,\nu} = 4 \left( \frac{t_{\nu,\nu}^2}{U^d} + 2 \frac{V_\nu^4}{U^d{}^3} \right) \quad (19)$$

where  $\vec{S}_i^\nu$  is the spin-1/2 operator for the spin degree of freedom associated with the electron in the  $\nu^{th}$   $d$ -orbital. The factor of 2 in the second term is due to the fact that there are two different paths, through the two different As atoms, which the superexchange mechanism can be materialized. On the other hand, for two next nn Fe atoms, such as 1 and 3 in Fig. 1, we obtain:

$$\mathcal{H}'_{\nu,\nu} = J'_{\nu,\nu} \sum_{\langle\langle ij \rangle\rangle} \vec{S}_i^\nu \cdot \vec{S}_j^\nu, \quad (20)$$

$$J'_{\nu,\nu} = \frac{4V_\nu^4}{U^d{}^3}. \quad (21)$$

There are contributions to the *effective hopping* matrix elements due to second order processes. Namely, processes in which an electron from a doubly occupied As orbital momentarily hops to the nn Fe  $d$  orbital and then an electron from the doubly occupied doped  $d$ -orbital

hops to the singly occupied As orbital left behind. As it has been already discussed each  $d$ -orbital hybridizes with a single As orbital (Table III) there are only diagonal effective hopping matrix elements, i.e.,

$$\delta t_{\nu,\nu} = \frac{V_\nu^2}{U_\nu^d}, \quad (22)$$

and we have neglected a small energy difference of the order of 0.2 eV which is small compared to the value of  $U_\nu^d$ . Therefore, the total matrix elements, for the case of nn Fe atoms (1 and 2 in Fig. 4), are given by

$$\tilde{t}_{\nu,\nu} = t_{\nu,\nu} + \frac{2V_\nu^2}{U_\nu^d}. \quad (23)$$

the second term is of the order of 0.4 eV for the cases of  $d_{xz}$  and  $d_{yz}$  and of the order of 0.1 eV for the  $d_{x^2-y^2}$ . In the case of next nn such as the Fe atoms 1 and 3 in Fig 4 we obtain

$$\tilde{t}'_{\nu,\nu} = \frac{V_\nu^2}{U_\nu^d}. \quad (24)$$

There is a direct hopping from a  $d_{xz}$  of one Fe atom to a  $d_{yz}$  orbital of a nn Fe atom and, similarly from  $d_{xy}$  to  $d_{z^2}$ . However, there is no second order contribution to these two effective hopping matrix elements because as can be verified from Table III there is no hybridization between these orbitals with the same As orbital. Thus, when  $\nu \neq \nu'$ ,

$$\tilde{t}_{\nu,\nu'} = t_{\nu,\nu'}, \quad (25)$$

$$\tilde{t}'_{\nu,\nu'} = 0, \quad (26)$$

where  $\nu, \nu'$  can be  $xz, yz$  and  $xy, z^2$ . Here,  $\tilde{t}'$  stands for hopping across two Fe atoms located on the diagonal of the square. Similarly, for these two cases we have only nn antiferromagnetic coupling as follows:

$$J_{\nu,\nu'} = \frac{4t_{\nu,\nu'}^2}{U^d}, \quad (27)$$

$$J'_{\nu,\nu'} = 0. \quad (28)$$

In summary, the Hilbert space of the effective low-energy hamiltonian separates into three sectors (a) the orbitals  $d_{xy}$  and  $d_{z^2}$  with 3 electrons occupied the two orbitals together (b) the orbitals  $d_{xz}$  and  $d_{yz}$  of each Fe atom which in the undoped case are occupied each by one electron. In the case of added electrons through doping these electrons lead to a double occupancy of these orbitals and these pairs of doubly occupied sites move through the lattice (c) the orbital  $d_{x^2-y^2}$ . The effective hamiltonian is given by

$$\begin{aligned} \mathcal{H}_{eff} &= \mathcal{H}_{xy,z^2} + \mathcal{H}_{xz,yz} + \mathcal{H}_{x^2-y^2,x^2-y^2} \\ &- J^H \sum_{i,\mu,\mu'} \vec{S}_i^\mu \cdot \vec{S}_i^{\mu'} \end{aligned} \quad (29)$$

where each of the  $H_{\mu,\mu'}$  terms above may be written as

$$\mathcal{H}_{\mu,\mu'} = - \sum_{\langle ij \rangle, \nu, \nu', \sigma} \tilde{t}_{\nu, \nu'} c_{j\nu' \sigma}^\dagger c_{i\nu \sigma} - \sum_{\langle\langle ij \rangle\rangle, \sigma, \nu} \tilde{t}'_{\nu, \nu} c_{j\nu \sigma}^\dagger c_{i\nu \sigma} + \sum_{\langle ij \rangle, \nu, \nu'} J_{\nu, \nu'} \vec{S}_i^\nu \cdot \vec{S}_j^{\nu'} + \sum_{\langle\langle ij \rangle\rangle, \nu} J'_{\nu, \nu} \vec{S}_i^\nu \cdot \vec{S}_j^\nu, \quad (30)$$

TABLE IV: The estimated matrix elements for the subspace of  $d_{xy}$  and  $d_{z2}$ .

	$\tilde{t}$	$\tilde{t}'$	$J$	$J'$
$d_{xy} \rightarrow d_{xy}$	0.12	0	0.01	0
$d_{z2} \rightarrow d_{z2}$	0.45	0.18	0.06	0.026
$d_{xy} \rightarrow d_{z2}$	0.08	0	0.005	0

TABLE V: The estimated matrix elements for the subspace of  $d_{xz}$  and  $d_{yz}$ .

	$\tilde{t}$	$\tilde{t}'$	$J$	$J'$
$d_{xz} \rightarrow d_{xz}$	0.55	0.2	0.08	0.03
$d_{yz} \rightarrow d_{yz}$	0.55	0.2	0.08	0.03
$d_{xz} \rightarrow d_{yz}$	0.3	0	0.07	0

where the possible values of  $\nu$  and  $\nu'$  are  $\mu$  and  $\mu'$  and correspond to the  $xz, yz$  and  $xy, z^2$  and for the case of the single orbital  $x^2 - y^2$  there is only the case where  $\mu = \mu' = x^2 - y^2$ .

Now we would like to give estimates of the couplings involved in the above model based on the values of the parameters obtained from fitting the LDA results to the tight binding model. The matrix elements for nn hopping  $\tilde{t}$  and spin-spin interaction  $J$  as well as their counterparts for next nn interactions (i.e., between sites diagonally across in the square lattice formed by the Fe atoms)  $\tilde{t}'$  and  $J'$  are given in Tables IV, V and VI for the cases of the three subspaces. In these estimates we have used  $U_\nu^d = 5$  eV.

#### IV. DISCUSSION

The three subsystems, which are described by the three separate hamiltonians, are characterized by different electron occupation numbers and this combined with the difference in the strengths of the  $\tilde{t}, \tilde{t}', J, J'$  implies that each sector can be in a different phase.

As can be observed from the atomic limit depicted in Fig. 4, at first, it appears that the  $d_{x^2-y^2}$  state and the  $d_{xz}, d_{yz}$  subspace are degenerate. However, both the hopping integrals and the exchange interactions characteriz-

TABLE VI: The estimated matrix elements for the subspace of  $d_{x^2-y^2}$ .

	$\tilde{t}$	$\tilde{t}'$	$J$	$J'$
$d_{x^2-y^2} \rightarrow d_{x^2-y^2}$	0.25	0.025	0.03	0

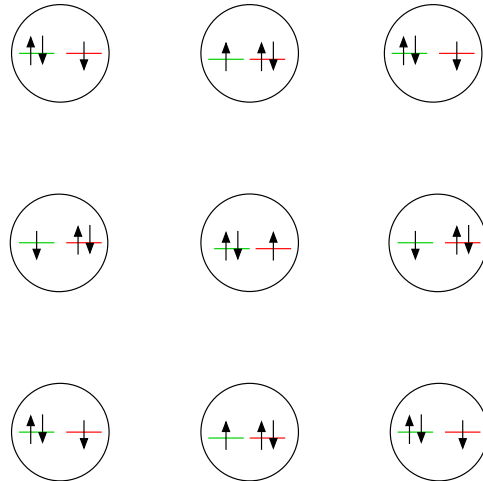


FIG. 5: The spin configuration of the nearest neighbor  $\text{Fe}^{2+}$   $d_{xz}$  and  $d_{yz}$  orbitals in the undoped parent compound. The green (red) line represents the  $d_{xz}$  ( $d_{yz}$ ) orbital within the same Fe atom.

ing the  $d_{xz}, d_{yz}$  subspace are significantly larger (compare Tables IV, V, VI) than the corresponding parameters in the other two subspaces. Furthermore, the energy difference between these atomic orbitals is smaller than these hopping matrix elements; therefore, the two bands corresponding to the subspace  $d_{xz}, d_{yz}$  are expected to be lower than those formed by the states of the other two subspaces.

We consider the undoped case first. The subspace spanned by  $d_{xz}$  and  $d_{yz}$  is occupied by 3 electrons per Fe site while the subspace spanned by  $d_{xz}$  and  $d_{yz}$  and the one spanned by  $d_{x^2-y^2}$  contains one electron per site per orbital. In the former subspace alone, we expect the spin configuration shown in Fig. 5 to optimize the energy for some appropriate value of  $J^H$ . This configuration allows nn hopping of the doubly occupied sites between the same Fe orbitals because the number of doubly occupied orbitals do not change through this process. The effective hopping between different type ( $d_{xz} \rightarrow d_{yz}$ ) nn Fe orbitals is smaller than the effective hopping between the same type nn Fe orbitals and, in addition, the former hopping process increases the number of doubly occupied orbitals. This configuration encourages the latter process which leads to significant lowering of the energy and discourages the former. In addition, the orientations of the net spin along one direction (the horizontal direction, in

Fig. 5) and those along the diagonal of the square are antiferromagnetically aligned; furthermore, along the other direction (vertical direction in Fig. 5), the orientations of the net spin are ferromagnetically aligned. Given the constraint that we have 3 electrons per two such orbitals, it is not possible to have non-zero net spin in both orbitals and this particular arrangement clearly does a good job in terms of minimizing the energy. Notice that the ferromagnetic arrangement of spins of electrons belonging to different orbitals does not hinder electron hopping and, in addition, the hopping occurs in harmony with the Hund's rule coupling. In fact the observed SDW order described in Ref. 26, which is depicted in Fig. 1, is consistent with that described in Fig. 5. This state occurs at temperature below the critical temperature for the distortion from the tetragonal to monoclinic.

We emphasize that unlike the case of undoped cuprates, the undoped parent compound in the case of the oxypnictides is not an insulator. As can be inferred from Fig. 5, the motion along the ferromagnetic direction is not hindered and, therefore, the undoped material is expected to demonstrate anisotropic transport in the SDW phase.

The other two subspaces, however, are half-filled and, therefore, we expect that a long-range antiferromagnetic order would characterize the ground state of these subspaces if they were uncoupled from the first subsystem. However, due to Hund's rule represented by the coupling  $J^H$  alone, the spin orientation of all subspaces should be common. This somewhat different "desires" preferred by the three subsystems (which are forced to make a common choice) introduces frustration of relative spin orientation.

The phenomenological hamiltonian, considered in Ref. 16,17 and in Ref. 21 to introduce frustration, is very different from the one we derived based on a more rig-

orous approach. In addition, we find that the state depicted in Fig. 5 while in agreement with experiment, it is qualitatively different than that considered in the above two papers. The next step is to study the hamiltonian (29,30) by various numerical techniques.

Since the estimated antiferromagnetic coupling constants are smaller than the one in the cuprous oxides<sup>32</sup> and in addition there is some degree of frustration (with the exception of the coupling between  $d_{xz} - d_{yz}$ ) as discussed we might initially feel that the pairing energy scale is also down relative to that in the cuprate superconducting materials. However, the binding energy scale in the present model may be enhanced by the "flavor" factor, i.e., the number of states spanning the subspace where the added electrons go (in the case of electron doping), and by the fact that the hopping matrix elements are estimated to be somewhat larger than the case of the cuprates (See Tables IV,V,VI). Therefore, it is conceivable that this new class of superconductors could lead to higher critical temperatures upon future optimization of the doping agents and other factors.

A very important difference between the oxypnictides and the cuprates is that the five-fold sector separates into three subsectors, two two-flavor sectors and a third with a single flavor. The lowest energy sector prefers the SDW order depicted in Fig. 5 while the other two prefer antiferromagnetic long-range order. These subspaces are coupled by Hund's rule which leads to a compromise SDW order with ferromagnetic along one dimension and antiferromagnetic ordering between such chains. As in the case of cuprates, in the present family of materials, superconductivity might coexist with SDW order<sup>33</sup> but these are expected to be to some extent competing orders as found in neutron<sup>34</sup> and  $\mu SR$  studies<sup>35</sup> from the superconducting doped materials.

- 
- <sup>1</sup> Y. Kamihara, et al., *J. Am. Chem. Soc.* **128**, 10012 (2006).  
<sup>2</sup> Y. Kamihara, et al., *J. Am. Chem. Soc.* **130**, 3296 (2008).  
<sup>3</sup> Z.-A. Ren et al., arXiv:0803.4283, and arXiv:0804.2053.  
 Z.-A. Ren et al., *Chin. Phys. Lett.* **25**, 2215 (2008).  
<sup>4</sup> X. H. Chen, et al., arXiv:0803.3603v1.  
<sup>5</sup> G. F. Chen, et al., arXiv:0803.3790v2.  
<sup>6</sup> H. H. Wen, et al., *Europhys. Lett.* **82**, 17009 (2008).  
<sup>7</sup> D. J. Singh and M.-H. Du, arXiv:0803.0429.  
<sup>8</sup> I.I. Mazin et al., arXiv:0803.2740.  
<sup>9</sup> K. Haule, J. H. Shim, and G. Kotliar, arXiv: 0803.1279.  
<sup>10</sup> L. Boeri et al., arXiv:803.2703.  
<sup>11</sup> C. Cao et al., arXiv:0803.3236v1.  
<sup>12</sup> B.-L. Yu et al. arXiv:0804.4028.  
<sup>13</sup> K. Kuroki et al., arXiv:0803.3325.  
<sup>14</sup> Z.-J Yao et al., arXiv:0804.4166.  
<sup>15</sup> X.-L Qi et al., arXiv:0804.4332.  
<sup>16</sup> T. Yildirim, arXiv:0804.2252.  
<sup>17</sup> F. Ma et al. , arXiv:0804.3370v2  
<sup>18</sup> S. Raghu et al., arXiv:0804.1113v1.  
<sup>19</sup> P. A. Lee and X.-G. Wen, arXiv:0804.1739.  
<sup>20</sup> V. Cvetkovic and Z. Tesanovic, arXiv:0804.4678.  
<sup>21</sup> C. Xu, M. Mueller, and S. Sachdev, arXiv:0804.4293.  
<sup>22</sup> Z.-Y. Weng, arXiv:0804.3228.  
<sup>23</sup> J. Li and Y. Wang, arXiv:0805.0644.  
<sup>24</sup> K. Haule and G. Kotliar, arXiv:0805.0722.  
<sup>25</sup> J. Dong et al., arXiv:0803.3426v1.  
<sup>26</sup> C. de la Cruz, et al., arXiv:0804.0795.  
<sup>27</sup> H.-H. Klauss et al., arXiv:08050264v1.  
<sup>28</sup> J. M. Soler, E. Artacho, J. D. Gale, A. García, J. Junquera, P. Ordejón, and D. Sánchez-Portal, *J. Phys.: Condens. Matter* **14**, 2745 (2002).  
<sup>29</sup> N. Troullier, and J. L. Martins, *Phys. Rev. B* **43**, 1993 (1991).  
<sup>30</sup> D. M. Ceperley, B. J. Alder, *Phys. Rev. Lett.* **45**, 566 (1980).  
<sup>31</sup> J. H. Jefferson, *J. Phys. C* **21**, L193 (1988).  
<sup>32</sup> E. Manousakis, *Rev. Mod. Phys.* **63**, 1 (1991).  
<sup>33</sup> A. J. Drew, et al., arXiv:0805.1042.  
<sup>34</sup> Y. Qiu, et al., arXiv:0805.1062v1.  
<sup>35</sup> J. P. Carlo et al., arXiv:0805.2186v1.